$CoSi_2$ heteroepitaxy on patterned Si(100) substrates

O. P. Karpenko and S. M. Yalisove
Department of Materials Science and Engineering, University of Michigan, 2300 Hayward Street, Ann Arbor, Michigan 48109-2136

(Received 6 May 1996; accepted for publication 20 August 1996)

The influence of starting surface topography on the nucleation and growth of epitaxial silicide layers was investigated. $CoSi_2$ layers were grown via the template technique on one-dimensionally patterned Si(100) substrates. These substrates contained mesa stripes, running parallel to Si[011], and exhibited either a number of Si $\{hkl\}$ facets, or "smoothly varying" sinusoidal profiles. Conventional plan view and high resolution cross section transmission electron microscopy showed that the orientation and morphology of the $CoSi_2$ grains depend on the angle (θ) between the $CoSi_2$/Si interface normal and Si(100). $CoSi_2$(100) grains nucleated on mesa tops and trench bottoms, where $\theta<5°$, and formed atomically sharp interfaces. $CoSi_2$(110) and $CoSi_2$(221) grains nucleated along sidewalls of the mesa structures, in regions where $5°<\theta<11°$ and $\theta>5°$, respectively. $CoSi_2$(110) grains formed highly stepped interfaces with the substrate which were punctuated by step bunches at the grain boundary/substrate triple points. $CoSi_2$(221) grains formed rough interfaces with the substrate which were punctuated by facets and *B*-type silicide/substrate interfaces along Si{111} planes. Analysis of these data suggests that nucleation of $CoSi_2$(110) grains is associated with the presence of double height steps and step bunches with small surface misorientation, and that nucleation of $CoSi_2$(221) grains is associated with Si{111} facets, Si{311} facets, and step bunches with larger surface misorientation. © *1996 American Institute of Physics.* [S0021-8979(96)07222-2]

I. INTRODUCTION

Many questions still remain unanswered concerning the nucleation and growth of epitaxial films. One specific question addresses the nucleation of different epitaxial orientations of the same phase. In theory, reasons for the nucleation of different epitaxial orientations should be relatively simple to identify as nucleation is driven by the reduction in a specific component of system energy.[1,2] Experimentally, reasons for the nucleation of different epitaxial orientations are difficult to determine or verify. In order to determine the effect of a specific variable on heterogeneous nucleation, it is necessary to minimize (ideally, eliminate) the effect of all other variables in the experiment. Nevertheless previous studies have identified several factors affecting epitaxial nucleation. These include, but are not limited to, surface topography,[3–6] details of intermediate phase formation,[7] details of deposition,[3,8,9] as well as strain energy and coincidence site density.[10]

$CoSi_2$ on Si(100) is an example of a system where surface topography has been linked to the nucleation of different epitaxial orientations of the same phase.[3] For heteroepitaxy on Si(100), $CoSi_2$, a metal with a CaF_2 crystal structure (a_0 = 0.536 nm), grows with the following primary epitaxial orientation: $CoSi_2$(100)//Si(100) [referred to as $CoSi_2$(100)].[3,8] Two secondary epitaxial orientations have also been identified: $CoSi_2$(110)//Si(100) (Refs. 3, 8, and 10) [referred to as $CoSi_2$(110)] with two in-plane rotational variants, and $CoSi_2$ $\{22\bar{1}\}$//Si(100) (Refs. 10–12) [referred to as $CoSi_2$(221)] with four in-plane rotational variants. Table I summarizes the crystallographic relationship of each $CoSi_2$ epitaxial orientation relative to the Si(100) substrate. Previously, it was shown that by using an optimized template technique, singly oriented $CoSi_2$(100) films could be grown on flat Si(100) surfaces.[3] However, use of the same optimized template technique resulted in silicide films containing ~95% $CoSi_2$(110) for growth on macroscopically rough Si(100) surfaces.[3] Similarly, growth of $CoSi_2$ on Si(100) wafers taken from different wafer batches also resulted in films containing different volume fractions of $CoSi_2$(100) and $CoSi_2$(110).[13] Other studies have shown that $CoSi_2$(221) nucleation is associated with growth on higher indexed Si surfaces including Si {211} and Si {311},[11] and on faceted Si (100) surfaces.[12] All of these data point to surface topography as a dominant influence in the nucleation of different $CoSi_2$ epitaxial orientations. However, in order to better understand the role of surface topography in $CoSi_2$/Si heteroepitaxy, a more systematic study is needed.

This study has focused on identifying the effect that starting surface topography has on the nucleation of $CoSi_2$ on Si. To accomplish this goal, $CoSi_2$ was grown using a template technique[3] on patterned Si(100) substrates containing either a number of high indexed Si $\{hkl\}$ surfaces,[14] or "smoothly varying" sinusoidal profiles.[15] The template technique was chosen as the deposition process for two reasons. First, silicide growth on flat Si(100) using an optimized template results in singly oriented $CoSi_2$(100) films of the highest structural quality.[3] Second, deposition of the silicide layer should not significantly alter the topography of the substrate starting surface.[16,17] The template is formed by room temperature deposition of thin (~0.2 nm) Co and Si layers followed by a brief anneal at $T < 470$ °C. Due to this low annealing temperature and to the fact that nearly all of the Co and Si were deposited in a stoichiometric ratio (only the first monolayer of Co was deposited without additional Si), all reactions should be confined to the top monolayer of sub-

TABLE I. $CoSi_2$ epitaxial orientations and their rotational variants on Si(100).

Out-of-plane orientation	In-plane orientation
$CoSi_2(100)//Si(100)$	$CoSi_2[011]//Si[011]$
$CoSi_2(110)//Si(100)$	$CoSi_2[001]//Si[011]$
	$CoSi_2[\bar{1}10]//Si[011]$
$CoSi_2(22\bar{1})//Si(100)$	$CoSi_2[\bar{1}10]//Si[011]$
	$CoSi_2[1\bar{1}0]//Si[011]$
	$CoSi_2[114]//Si[011]$
	$CoSi_2[\bar{1}\bar{1}\bar{4}]//Si[011]$

strate Si, and the topography of the substrate should not be significantly altered.[16,17] Since the epitaxial orientation of the $CoSi_2$ grains is determined at the start of growth, during template formation, microscopic analyses of the silicide/Si interface should reveal topographic features characteristic of each $CoSi_2$ epitaxial orientation, and could help identify potential nucleation sites for each silicide orientation. In order to insure that surface topography was the only variable affecting silicide nucleation, $CoSi_2$ was grown using an optimized template, described in detail in Sec. II, on both flat and patterned Si(100) substrates, taken from the same batch of wafers.[13] Since the template produced singly oriented $CoSi_2(100)$ films on flat Si(100), any change in the $CoSi_2$ film morphology or epitaxial orientation could be attributed solely to changes in surface topography between the flat and the patterned Si(100) substrates. The advantage of using patterned substrates was that each substrate contained a wide range of surfaces and surface topographical features. This provided a means by which to quickly evaluate the effect of surface topography on silicide nucleation, and eliminated many problems associated with reproducibility and analysis of films grown on different substrates.

II. EXPERIMENT

Patterned, boron doped, Si(100) wafers, $\rho \sim 0.2–0.4$ Ω cm, were prepared using conventional photolithography and plasma etching. Etching was performed with a rf generated plasma in a mixture of SF_6 and O_2. Following etching, the wafers were stripped of photoresist and degreased. These wafers contained mesa stripes that extended across the entire wafer surface in the Si[011] direction, with a periodicity of 4 μm, and a depth that varied from 100–300 nm (depending on the length of etching) [see Fig. 1(a)]. The wafers were then diced to appropriate sizes (0.25 in. × 1.20 in.), cleaned using a modified RCA cleaning procedure that left the substrates capped with a thin volatile oxide layer.[18] Substrates were introduced into a four chamber cryopumped molecular beam epitaxy (MBE) system ($P_{base} \sim 5.0$ E-11 Torr) via a mechanically pumped loadlock, and moved into a sample preparation chamber. In the sample preparation chamber, each substrate was outgassed for 15 min at 100 °C, 15 min at 300 °C, and 2 h at 550 °C. After outgassing, substrates were transferred into the growth and analysis chamber. The protective oxide layer was then thermally volatized by heating to ~1000 °C for 2 min. Substrates were then cooled to ~450 °C, and a 100 nm Si buffer layer was grown by electron beam evaporation of a solid Si source. Following Si buffer layer growth each substrate was annealed at ~950 °C for 1–3 h to achieve the desired surface profile. Shorter anneals produced substrates with a number of Si $\{hkl\}$ facets, including Si{711}, Si{511}, Si{311}, Si{111}, and Si(100) (Refs. 14 and 15) [see Fig. 1(b)]. Longer anneals produced substrates with smoothly varying sinusoidal profiles [see Fig. 1(c)]. The annealing process was monitored with *in situ* reflection high energy electron diffraction (RHEED) and low energy electron diffraction (LEED). Analysis of RHEED and LEED patterns helped determine anneal times and verify the presence of various facets on the substrate surface. After annealing, substrates were rapidly cooled to room temperature prior to silicide growth, and were analyzed with Auger electron spectroscopy to evaluate the cleanliness of the substrate surface.

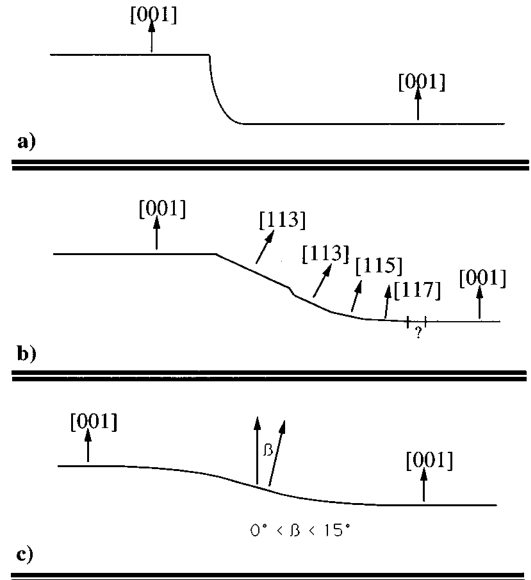

FIG. 1. Schematic diagram of the surface profile of a patterned Si(100) substrate. In all of the schematics, the Si[011] direction is normal to the page. (a) Si(100) substrate profile after plasma etching. (b) Si(100) substrate profile after plasma etching, 100 nm buffer layer growth at 650 °C, and annealing for 1 h at 950 °C. (c) Si(100) substrate profile after plasma etching, 100 nm buffer layer growth at 650 °C, and annealing for 2.5 h at 950 °C.

$CoSi_2$ layers were grown on the patterned Si substrates using an optimized template technique.[3] The template consisted of a room temperature deposition of 0.2 nm of Co, followed by codeposition of an additional 0.2 nm of Co in a stoichiometric ratio with Si (Co:Si=1:2). These layers were annealed to ~470 °C for 2 min to form the $CoSi_2$ template. With the substrate held at ~470 °C, the silicide films were thickened to ~10–20 nm by codeposition of Co and Si in a stoichiometric ratio. Both Co and Si were deposited via electron beam evaporation of solid sources. Deposition rates were monitored by quartz cantilevers and were calibrated with Rutherford backscattering spectroscopy and cross section high resolution electron microscopy. During deposition the pressure in the growth chamber remained below 1.0 E-9 Torr. After deposition, substrates were rapidly cooled to

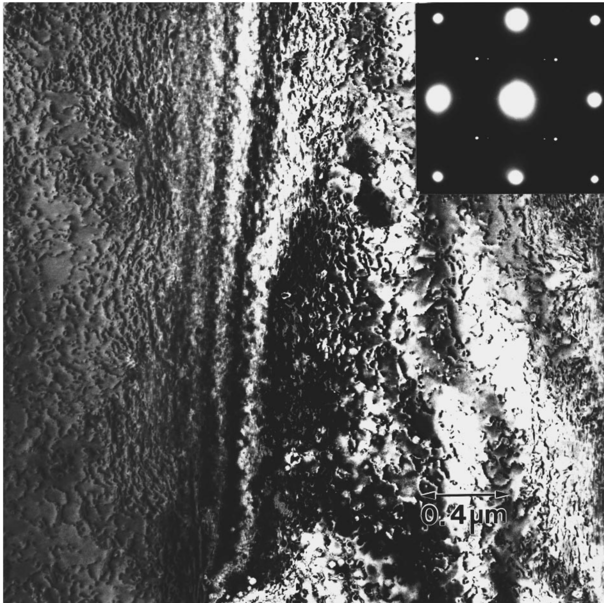

FIG. 2. Bright field plan view transmission electron micrograph, taken near the Si(100) zone axis, of a $CoSi_2$ film grown on a patterned Si(100) substrate. The inset in the upper right-hand corner shows a selected area diffraction pattern taken from this region of the substrate.

room temperature and removed from the MBE system for postgrowth analysis. All substrates were heated resistively by passing current directly through them.

The silicide films were analyzed using conventional plan view transmission electron diffraction and microscopy (TED and TEM, respectively), and cross-sectional high resolution transmission electron microscopy (HREM). Plan view TEM samples were prepared by ultrasonic cutting, mechanical thinning to ~125 μm, and chemical etching to perforation. Cross-sectional HREM samples were prepared by substrate cleavage, mechanical thinning to ~30 μm, polishing, and ion milling to perforation with 5 keV Ar^+ ions. Plan view TEM was performed using a Philips 420 T, operating at 120 kV. Cross-sectional HREM was performed using a JEOL 4000 EX, operating at 300 kV.

III. RESULTS

A. Plan view transmission electron diffraction and microscopy

Analysis of selected area (using an aperture size of ~10 μm) plan view transmission electron diffraction patterns of the $CoSi_2$ films grown on patterned Si(100) substrates suggests that the silicide grows with three epitaxial orientations. Diffraction patterns taken near the Si(100) zone axis (see inset, Fig. 2) suggest the following epitaxial orientations: $CoSi_2(100)//Si(100)$ with $CoSi_2(011)//Si(011)$, and one rotational variant of $CoSi_2(110)//Si(100)$ with $CoSi_2(001)//Si(0\bar{1}1)$. Diffraction patterns taken along other Si zone axes suggest one additional epitaxial orientation with two rotational variants: $CoSi_2(\bar{1}22)//Si(100)$ with $CoSi_2(411)//Si(0\bar{1}1)$, and $CoSi_2(\bar{1}22)//Si(100)$ with $CoSi_2(\bar{4}\bar{1}\bar{1})//Si(0\bar{1}1)$. From these diffraction patterns it was determined that *all* of the silicide grains were aligned with a $CoSi_2\langle 110\rangle$ direction parallel to the direction of the mesa stripes, Si[011]. Data concerning the location of the misoriented silicide grains were obtained by reducing the size of the electron probe and collecting microdiffraction patterns from various regions of the films. Microdiffraction patterns taken near mesa tops and trench bottoms show that in these regions $CoSi_2$ grows with only one epitaxial orientation, $CoSi_2(100)//Si(100)$. However, microdiffraction patterns taken near the sidewalls indicate that in these regions $CoSi_2$ grows with all three epitaxial orientations.

Plan view TEM micrographs taken near the Si(100) zone axis show that the silicide films are continuous, and that the defect density and epitaxial orientation of the $CoSi_2$ films vary with location along each mesa structure. Zone axis bright field micrographs (Fig. 2) indicate that $CoSi_2$, with a low defect density, grows on the mesa tops and trench bottoms, while along the sidewalls of the mesa structure the defect density in the silicide film dramatically increases. In order to locate the position of the misoriented $CoSi_2$ grains, and to verify the results of the microdiffraction analysis, bright field and dark field micrographs were taken using diffraction maxima from $CoSi_2$ grains of each epitaxial orientation. The position and density of $CoSi_2(100)$ grains were determined from two-beam bright field and dark field micrographs taken using $\mathbf{g}=200$, and $\mathbf{g}=200$ with a 200 diffraction maxima of $CoSi_2(100)$, respectively. These micrographs show that the mesa tops and trench bottoms contain exclusively $CoSi_2(100)$. The density and position of $CoSi_2(110)$ grains were determined from two-beam bright field [Fig. 3(a)] and dark field micrographs [Fig. 3(b)] taken using $\mathbf{g}=111$, and $\mathbf{g}=111$ with a 111 diffraction maxima of $CoSi_2(110)$, respectively. The density and position of $CoSi_2(221)$ grains were determined from two-beam bright field [Fig. 4(a)], and dark field micrographs [Fig. 4(b)], taken using $\mathbf{g}=311$, and $\mathbf{g}=311$ with a 311 diffraction maxima from $CoSi_2(221)$, respectively. These micrographs confirm that the $CoSi_2(110)$ and $CoSi_2(221)$ grains are most highly concentrated near the sidewalls of the mesa structure. They also indicate that the density of $CoSi_2(221)$ grains along the sidewalls of the mesa structure is higher than the density of $CoSi_2(110)$ grains. However, identification of specific nucleation sites for these misoriented grains was not possible. The plan view TEM micrographs also show that all of the grains along the sidewall are elongated in the direction of the mesa stripes.

B. High resolution cross-sectional transmission electron microscopy

Cross-sectional HREM analysis of the $CoSi_2$ films corroborated the plan view TEM/TED analyses, and provided additional information about the film morphology. Lattice images of the silicide films on patterned Si substrates confirmed the presence of all three epitaxial orientations indexed in the plan view TED patterns [$CoSi_2(100)$, one rotational variant of $CoSi_2(110)$, and two rotational variants of $CoSi_2(221)$]. Additionally, an alignment of a $CoSi_2\langle 110\rangle$ direction with the mesa stripe direction, Si[011], was observed in all $CoSi_2$ grains. The epitaxial orientation of each

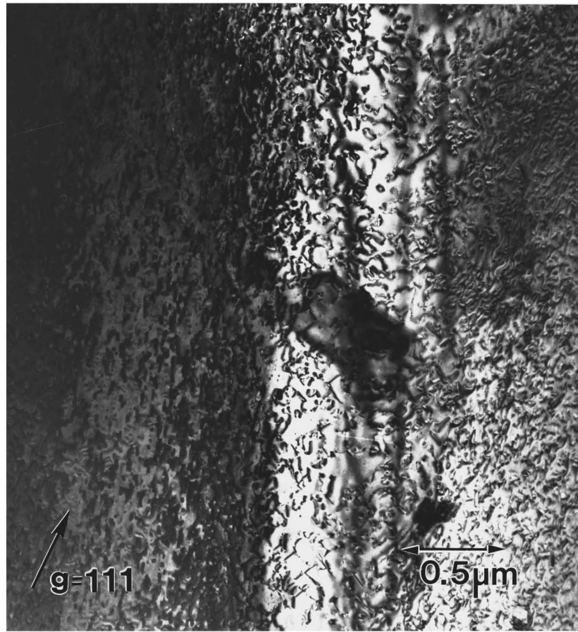

(a)

(b)

FIG. 3. Plan view transmission electron micrographs of a $CoSi_2$ film grown on a patterned Si(100) substrate. (a) Two-beam bright field micrograph taken with the transmitted beam and **g**=111 of the $CoSi_2(110)$ grains. (b) Dark field micrograph taken with a 111 diffracted beam of the $CoSi_2(110)$ grains and **g**=111 of the $CoSi_2(110)$ grains.

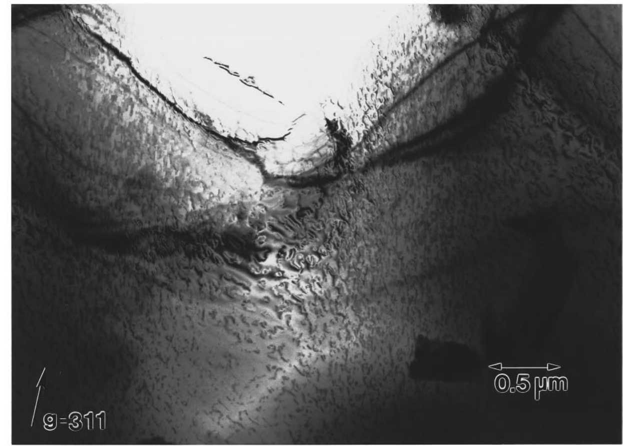

(a)

(b)

FIG. 4. Plan view transmission electron micrographs of a $CoSi_2$ film grown on a patterned Si(100) substrate. (a) Two-beam bright field micrograph taken with the transmitted beam and **g**=311 of the $CoSi_2(221)$ grains. (b) Dark field micrograph taken with a 311 diffracted beam of the $CoSi_2(221)$ grains and **g**=311 of the $CoSi_2(221)$ grains.

silicide grain relative to the Si substrate was determined by indexing simulated diffraction patterns of the lattice images. These diffraction patterns were produced by taking fast Fourier transforms of the $CoSi_2$/Si lattice images, and were used to map the location of $CoSi_2(100)$, $CoSi_2(110)$, and $CoSi_2(221)$ grains as a function of misorientation angle (θ), from Si(100) (Fig. 5). The plot in Fig. 5 was generated by calculating the linear fractions of $CoSi_2(100)$, $CoSi_2(110)$, and $CoSi_2(221)$ grains and plotting them versus θ, the angle measured between the $CoSi_2$/Si interface normal and Si(100). In total, 10 $CoSi_2$ films and a combined interface length in excess of ~ 40 μm were analyzed. In order to simplify the representation of this data, analysis of growth on all Si surfaces was included in the plot.

The results of the cross-sectional HREM analysis show that the $CoSi_2(100)$ grains grew predominantly at mesa tops and at trench bottoms (Fig. 6), in regions where $\theta < 5°$. These grains were large in size ($d > 250$ nm) and formed atomically sharp interfaces with the Si substrate. Close inspection of Fig. 6 reveals that, in regions of low misorientation, $CoSi_2(100)$ grains easily accommodated Si steps at the silicide/Si interface (these steps appear to be single height steps). Conversely, $CoSi_2(110)$ grains grew along the sidewalls of the mesa structures and had grain sizes ($d \approx 30$ nm) that were significantly smaller than those of the $CoSi_2(100)$ grains, as seen in the plan view TEM analysis. $CoSi_2(110)$ grains nucleated in regions where θ varied from 5° to 11°, and formed rough interfaces with the substrate (Fig. 7). Furthermore, in most ($\sim$90%) of the $CoSi_2(110)$ grains, the grain boundary/substrate triple points were punctuated by regions of step bunching. Similarly, $CoSi_2(221)$ grains grew

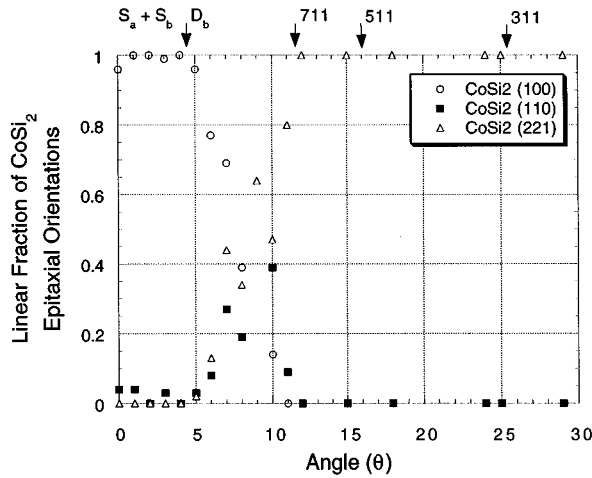

FIG. 5. Plot of the linear fractions of $CoSi_2(100)$, $CoSi_2(110)$, and $CoSi_2(221)$ grains as a function of θ, the angle measured between the $CoSi_2$/Si interface normal and Si(100). The plot includes data for growth on patterned substrates with both well defined Si $\{hkl\}$ surfaces and smoothly varying sinusoidal profiles. The plot does not include grains that nucleated at facet intersections.

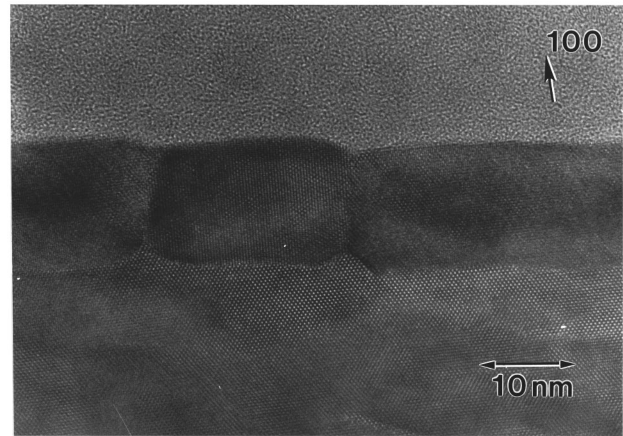

FIG. 7. Cross-sectional high resolution transmission electron micrograph showing a lattice image along a Si⟨110⟩ projection of a $CoSi_2(110)$ grain between two $CoSi_2(100)$. This silicide/substrate interface normal is misoriented ~5° from Si(100) in this region. The arrowheads in the micrograph point to facets and step bunches at the grain boundary/substrate triple points.

along the sidewalls of the mesa structures and also exhibited small grain sizes ($d \approx 25$ nm). These grains nucleated in regions where $\theta > 5°$ and dominated film growth in regions of high misorientation, $\theta > 12°$. $CoSi_2(221)$ grains also formed rough interfaces with the Si substrate. These interfaces were predominantly *B*-type interfaces along Si{111} planes (see Fig. 8). A *B*-type interface is described by a 180° rotation of the silicide lattice relative to the Si lattice, about a Si⟨111⟩ direction. $CoSi_2(221)$ grains were also found in relatively flat areas of the substrate on features with locally high misorientation (i.e., isolated step bunches or Si{311} facets) (see Fig. 9). Figure 9 shows a $CoSi_2(221)$ grain that appears to have nucleated on a step bunch between two relatively flat regions of the substrate containing $CoSi_2(100)$.

The high resolution cross-sectional TEM analysis of the $CoSi_2$ films also provided an opportunity to investigate the grain size dependence of $CoSi_2$ as a function of θ, the angle of misorientation from Si(100). The plot generated from this data (Fig. 10) shows a significant decrease in the silicide grain size with increasing misorientation from Si(100). This plot was generated from the cross-sectional HREM data rather than from the plan view TEM data in order to eliminate errors associated with measuring grain sizes on inclined surfaces. Comparison between the two data sets shows a qualitative agreement.

IV. DISCUSSION

Before attempting to analyze the above results, it would be useful to review what is known about Si surface topography, and determine which surface topographical features are likely to be present on the patterned Si(100) substrates. Keeping in mind that the substrates were patterned with mesa stripes along Si[011], and that steps on Si surfaces run along Si⟨110⟩ directions,[19,20] it is expected that steps on the patterned substrates will run predominantly along sidewalls, parallel to the mesas. In regions of low misorientation from Si(100), $\theta < 4°$, near mesa tops and trench bottoms, the patterned substrates should contain predominantly single height steps (for the purposes of this discussion, no distinction between S_a and S_b steps will be made).[19,20] As the surface misorientation increases above 5°, moving down a sidewall in the mesa structure, a transition from single height to

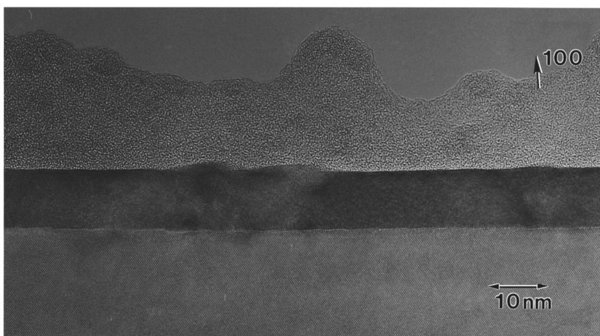

FIG. 6. Cross-sectional high resolution transmission electron micrograph showing a lattice image along a Si⟨110⟩ projection of a $CoSi_2$ layer grown on a patterned Si(100) substrate. The silicide layer is oriented with $CoSi_2(100)//Si(100)$. Note the steps along the silicide/substrate interface.

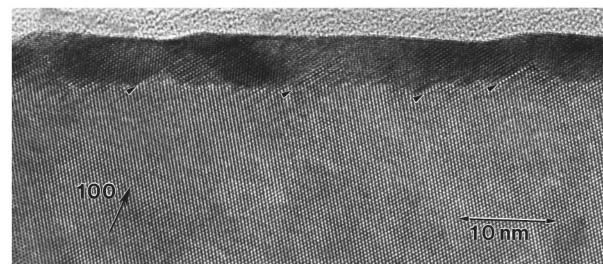

FIG. 8. Cross-sectional high resolution transmission electron micrograph showing a lattice image along a Si⟨110⟩ direction of several $CoSi_2(221)$ grains. The arrowheads in the micrograph point to facets at the silicide/substrate interface, along Si{111} planes. The silicide/substrate interface normal is misoriented ~24° from Si(100) in this region.

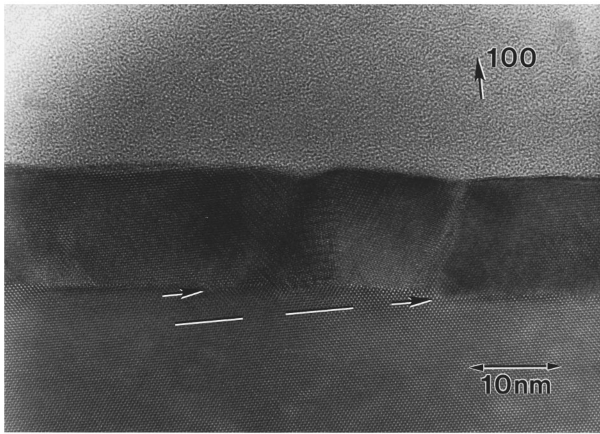

FIG. 9. Cross-sectional high resolution transmission electron micrograph showing a lattice image along a Si⟨110⟩ direction of a $CoSi_2(221)$ grain that has nucleated on a Si step bunch between two relatively flat regions of the substrate containing $CoSi_2(100)$.

double height steps should occur.[19–21] A further increase in surface misorientation should result in the formation of stable facets and surfaces such as Si{711}, Si{511}, Si{311}, and Si{111}.[14,22–25] Unfortunately, most of these higher indexed surfaces have complex structures that have not yet been fully determined. Past work has shown that Si{511} (Ref. 26) and Si{311} (Refs. 27–32) surfaces are reconstructed, and are not simply made up of small Si(100) terraces separated by double height steps, as may be the case with Si{711} surfaces.[33] It is also possible that these higher indexed surfaces contain small facets of other orientations (i.e., Si{111}, Si{311}).[34,35] Indeed, a recent study has shown that Si surfaces vicinal to Si{211} contain a high density of {111} nanoscale facets.[35] Additionally, the surfaces of the patterned wafers were annealed at high temperatures for extended periods prior to silicide growth. During this annealing process, step motion on the substrate surface, coupled with the presence of pinning sites (i.e., impurities), could induce the formation of step bunches, as well as Si{311} facets.[27]

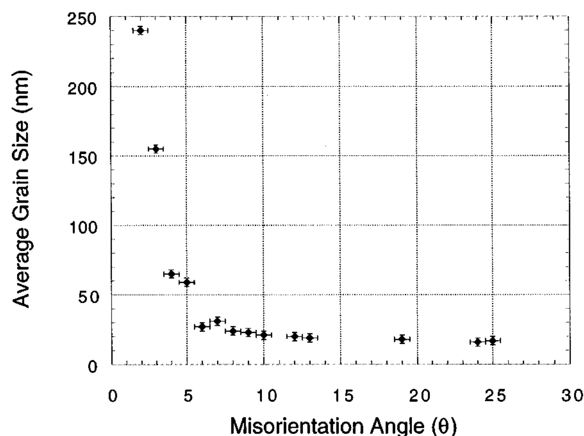

FIG. 10. Plot of the average $CoSi_2$ grain size as a function of misorientation from Si(100). The plot was generated by plotting the average grain size of the silicide grains vs θ, the angle measured between the $CoSi_2$/Si interface normal and Si(100).

Furthermore, the high temperature annealing step should result in surface smoothing and in the elimination of surface roughness associated with multilayered islanded structures. In summary, it is expected that the surfaces of the patterned substrates contain (1) single and double height steps running parallel to the mesa stripes, (2) stable high indexed Si $\{hkl\}$ surfaces, (3) nanoscale facets (probably Si{111}) on the high indexed Si $\{hkl\}$ surfaces, and (4) regions of step bunching.

In light of the above discussion, the heteroepitaxial growth of $CoSi_2$ on patterned Si substrates can be analyzed, and possible nucleation sites for each $CoSi_2$ epitaxial orientation can be suggested. One interesting feature of the plan view TED/TEM data is the presence of only one rotational variant of $CoSi_2(110)$ and two rotational variants of $CoSi_2(221)$, as compared to two variants of $CoSi_2(110)$ and four variants of $CoSi_2(221)$ for growth on nominally flat Si(100) surfaces. This observation implies that the nucleation of misoriented $CoSi_2$ grains is related to the symmetry of surface step structure on the substrate. By artificially constraining steps to run predominantly along one Si⟨110⟩ direction (Si[011], parallel to the mesas) on patterned substrates, as opposed to along two orthogonal Si⟨110⟩ directions, as on nominally flat Si(100) surfaces, the number of rotational variants of misoriented $CoSi_2$ grains was reduced by a factor of 2.

The plan view TED/TEM data also show an alignment of $CoSi_2$ grains with Si[011]. Along this direction the silicide grains are elongated, grow with a $CoSi_2$⟨110⟩ direction parallel to Si[011], and have favorable lattice matching, −1.2%. However, along Si[$0\bar{1}1$], the direction moving down the sidewall of the mesa structures and across step edges, the silicide grain dimensions are smaller. The lattice mismatch for the $CoSi_2(110)$ grains is also considerably worse, +4.7%. These data imply that the nucleation of misoriented grains is related to the symmetry of the initial surface step structure, and epitaxy is disrupted by the presence of step edges. Epitaxial growth along steps resulted in large grain dimensions and favorable lattice matching, while growth across steps resulted in reduced grain dimensions and, in the case of $CoSi_2(110)$ grains, poor lattice matching with the Si substrate. Since cross-sectional HREM micrographs suggest that single height steps do not appear to hinder $CoSi_2$ heteroepitaxy (cf. Fig. 6), this points to double height steps and larger scale surface topographical features (i.e., facets, step bunches) as dominant influences in the nucleation of misoriented silicide grains.

Analysis of cross-sectional HREM data was used to help identify possible nucleation sites for the misoriented $CoSi_2$ grains. As already mentioned, $CoSi_2$ growth using the template technique should not significantly alter the structure of the starting Si surface, although limited mass transport in the top monolayer of Si is expected.[17] Previous work has already demonstrated that silicide growth of $CoSi_2$ on Si(111) preserves the surface step structure of the substrate at room temperature,[16] but does result in slight alterations of the surface step structure at $T \sim 450\,°\mathrm{C}$.[17] Similar behavior is expected for growth on Si(100). Due to the low growth temperatures and the stoichiometry of the deposited material

(only the first monolayer of Co can react with the substrate) used in this study, mass transport between the deposited material and the substrate should be limited to the top monolayer of substrate Si, and some signature of the nucleation sites for each misoriented silicide grain should remain. The HREM micrographs show that $CoSi_2(110)$ grains are bounded by regions of step bunching at the grain boundary/substrate triple points. Although these features are seen in nearly all (~90%) of the $CoSi_2(110)$ grains, their final morphology could be influenced by mass transport driven by balancing of interfacial and grain boundary energies between $CoSi_2(100)$, $CoSi_2(110)$, $CoSi_2(221)$, and the Si substrate.[35] Based solely on the HREM data, it is not possible to firmly establish the role of microfacets and step bunches in the nucleation of $CoSi_2(110)$ grains. Additional information on possible nucleation sites for $CoSi_2(110)$ grains is provided in Fig. 5. This plot shows that the density of $CoSi_2(110)$ grains rapidly increases at $\theta > 5°$, a value of surface misorientation where one would expect to see double height steps and step bunches with low misorientation from Si(100). Although the association of $CoSi_2(110)$ grains with the presence of double height steps and small step bunches on the Si surface is strongly suggested by the data, this cannot be confirmed without further experiments [e.g., analysis of $CoSi_2$ heteroepitaxy on Si(100) substrates miscut ~5° towards Si⟨011⟩]. Nevertheless, speculation that these surface topographical features are linked to $CoSi_2(110)$ nucleation, perhaps by providing a more favorable geometrical lattice match and a lower strain energy density than flat Si(100),[10] is consistent with past work and with the observations and arguments mentioned above (double height step edges and larger scale surface topographical features might be linked to the nucleation of misoriented $CoSi_2$ grains).

Possible nucleation sites for $CoSi_2(221)$ grains are also suggested by direct inspection of cross-sectional HREM micrographs. These nucleation sites include Si{111} facets, Si{311} facets, and step bunches with high misorientation from Si(100). HREM micrographs of $CoSi_2(221)$ grains show a high density of *B*-type interfaces with the substrate along Si{111} planes (see Fig. 8). Other micrographs show that $CoSi_2(221)$ grains grow along Si{311} facets and on step bunches along the Si surface (see Fig. 9). In many cases these grains also formed *B*-type interfaces with the substrate along Si{111} interfacial facets. This is not surprising for two reasons. First, the $CoSi_2(221)$ epitaxial orientation is crystallographically related to Si(100) by a *B*-type interface along an off-normal Si⟨111⟩ direction. Second, the formation of *B*-type $CoSi_2$/Si interfaces is expected for this particular $CoSi_2$ template along Si{111} surfaces.[17,36–39] Similarly, due to a good geometrical lattice match and overall low interfacial energy, the growth of $CoSi_2(221)$ along Si{311} surfaces can be explained in terms of the minimization of interfacial energy between $CoSi_2$ and Si due to the formation of *B*-type interfaces along Si{111} facets at the silicide/Si interface.[11] From these data it is clear that the formation of Si{111} facets and *B*-type interfaces are important to the nucleation of $CoSi_2(221)$ grains. Furthermore, it is unlikely that these facets form as a result of deposition because mass transport is limited to the top monolayer of the Si substrate, and Si{111} and Si{311} facets are expected along higher indexed Si {*hkl*} surfaces. For these reasons it is speculated that nucleation sites are limited to Si{111} facets and surface topographical features that closely resemble Si{111}, including step bunches with large misorientations from Si(100), and large surface corrugations and roughness on high indexed Si {*hkl*} facets.

V. SUMMARY

This study has demonstrated that surface topography alone can induce the nucleation of variously oriented $CoSi_2$ grains on patterned Si(100) substrates. These results suggest possible nucleation sites for both $CoSi_2(110)$ and $CoSi_2(221)$ grains, and have provided additional information on the effect of surface topography in $CoSi_2$/Si heteroepitaxy. The approach used in this study involved silicide growth, using an optimized template technique, on patterned Si(100) substrates that contained mesa stripes, parallel to Si[011], and a wide variety of surface topographical features. Since the template technique utilizes low growth temperatures, the interface between the silicide and the substrate should be topographically similar to the starting substrate surface. Hence, microscopic analyses should help determine possible nucleation sites for each silicide orientation. Indeed, microscopic analyses revealed that the epitaxial orientation and morphology of $CoSi_2$ grains had a strong dependence on the misorientation between Si(100) and the silicide/substrate interface normal. $CoSi_2(100)$ grew in relatively flat regions of the substrate ($\theta < 5°$), where single height steps should be the dominant surface topographical features. $CoSi_2(110)$ grains were found in regions of slightly higher surface misorientation ($5° < \theta < 12°$). These data suggest that $CoSi_2(110)$ nucleation is linked to double height steps and small step bunches on the Si surface, perhaps due to more favorable geometric lattice matching than on flat Si(100). $CoSi_2(221)$ grains were found to dominate growth in regions of high surface misorientation ($\theta > 5°$), wherever silicide grains were able to form *B*-type interfaces along Si{111} planes. These data suggest that $CoSi_2(221)$ nucleation is linked to Si{111} facets, Si{311} facets, and large step bunches along the substrate surface.

The symmetry of the surface step structure was also found to influence silicide nucleation and growth. Growth on one-dimensionally patterned substrates resulted in half the number of rotational variants as typically found for growth on flat Si(100) substrates. This was attributed to the fact that steps run predominantly along one in-plane Si⟨110⟩ direction, parallel to the mesa stripes, on the patterned substrates, as opposed to two in-plane Si⟨110⟩ directions as on flat Si(100) substrates. Furthermore, epitaxial growth of the silicide grains parallel to mesa stripes (along step edges) resulted in large grain dimensions and favorable lattice matching (all silicide grains shared a common $CoSi_2⟨110⟩$ direction with the direction of the Si mesas, Si[011]). In contrast to this, growth normal to the direction of the mesas (across step edges) resulted in smaller grain dimensions and poorer lattice matching. These data seem to suggest that growth across step edges disrupted epitaxial growth, whereas growth along step edges facilitated epitaxial growth.

ACKNOWLEDGMENTS

The authors would like to thank David Adams and David Eaglesham for useful discussions, Jeff Kempisty for assistance in preparing the patterned Si substrates, Raymond Tung for valuable suggestions, and John Mansfield and the University of Michigan Electron Microbeam Analysis Laboratory for providing trouble-free use of the JEOL 4000 EX. This work was supported by the National Science Foundation, Contract No. DMR-9202176.

[1] D. A. Porter and K. E. Easterling, *Phase Transformations in Metals and Alloys* (Chapman and Hall, New York, 1981).
[2] K.-N. Tu, J. W. Mayer, and L. C. Feldman, *Electronic Thin Film Science for Electrical Engineers and Materials Scientists* (Macmillan, New York, 1992).
[3] S. M. Yalisove, R. T. Tung, and D. Loretto, J. Vac. Sci. Technol. A **7**, 1472 (1989).
[4] M. Sosnowski, S. Ramac, W. L. Brown, and Y. O. Kim, Appl. Phys. Lett. **65**, 2943 (1994).
[5] P. A. Bennett, S. A. Parikh, and D. G. Cahill, J. Vac. Sci. Technol. A **11**, 1680 (1993).
[6] M. Copel and R. M. Tromp, Appl. Phys. Lett. **65**, 3102 (1994).
[7] H. Sirringhaus, N. Onda, E. Muller-Gubler, P. Muller, R. Stadler, and H. von Kanel, Phys. Rev. B **47**, 10567 (1993).
[8] J. R. Jimenez, L. J. Schowalter, L. M. Hsuing, K. Rajan, S. Hashimoto, R. D. Thompson, and S. S. Iyer, J. Vac. Sci. Technol. A **8**, 3014 (1990).
[9] Y.-F. Hsieh, R. Hull, A. E. White, and K. T. Short, Appl. Phys. Lett. **58**, 122 (1991).
[10] C. W. T. Bulle-Lieuwma, A. H. van Ommen, J. Hornstra, and C. N. A. M. Aussems, J. Appl. Phys. **71**, 2211 (1992).
[11] J. M. Phillips, J. L. Batstone, J. C. Hensel, I. Yu, and M. Cerullo, J. Mater. Res. **5**, 1032 (1990).
[12] K. Rajan, L. M. Hsiung, J. R. Jimenez, L. J. Schowalter, K. V. Ramanathan, R. D. Thompson, and S. S. Iyer, J. Appl. Phys. **70**, 4853 (1991).
[13] S. M. Yalisove and R. T. Tung (unpublished). For a given template, it was found that the density of $CoSi_2(110)$ grains varied for growth on wafers taken from different wafer lots.
[14] D. P. Adams and S. M. Yalisove, Mater. Res. Soc. Symp. Proc. **317**, 35 (1994).
[15] W. W. Mullins, J. Appl. Phys. **28**, 333 (1957).
[16] R. T. Tung and F. Schrey, Phys. Rev. Lett. **63**, 1277 (1989).
[17] C. W. T. Bulle-Lieuwma and D. E. W. Vandenhoudt, J. Appl. Phys. **73**, 3220 (1993).
[18] A. Ishizaka and Y. Shiraki, J. Electrochem. Soc. **133**, 66 (1986).
[19] Ellen D. Williams and N. C. Bartelt, Science **251**, 393 (1991).
[20] D. J. Chadi, Phys. Rev. Lett. **59**, 1691 (1987).
[21] Z. Zhang, Y.-T. Lu, and H. Metiu, Phys. Rev. B **46**, 1917 (1992).
[22] D. G. Vlachos, L. D. Schmidt, and R. Aris, Phys. Rev. B **47**, 4896 (1993).
[23] R. J. Phaneuf and E. D. Williams, Phys. Rev. Lett. **58**, 2563 (1987).
[24] A. G. Schrott and J. M. Blakely, Surf. Sci. Lett. **150**, L77 (1985)
[25] C. C. Umbach, M. E. Keefe, and J. M. Blakely, J. Vac. Sci. Technol. A **9**, 1014 (1991).
[26] B. Z. Olshanetsky and V. I. Mashanov, Surf. Sci. **111**, 414 (1981).
[27] Y.-N. Yang and E. D. Williams, J. Vac. Sci. Technol. A **8**, 2481 (1990).
[28] W. Ranke, Phys. Rev. B **41**, 5243 (1990).
[29] J. Knall, J. B. Pethica, J. D. Todd, and J. H. Wilson, Phys. Rev. Lett. **66**, 1733 (1991).
[30] J. H. Wilson, P. D. Scott, J. B. Pethica, and J. Knall, J. Phys., Condens. Matter **3**, 5133 (1991).
[31] D. J. Chadi, Phys. Rev. B **29**, 785 (1984).
[32] A. Oshiyama, Phys. Rev. Lett. **74**, 130 (1994).
[33] H. Hirayama, M. Hiroi, and T. Ide, Phys. Rev. B **48**, 17331 (1993).
[34] H. Hibino , Y. Homma, and T. Ogino, Phys. Rev. B **51**, 7753 (1995).
[35] A. A. Baski and L. J. Whitman, Phys. Rev. Lett. **74**, 956 (1995).
[36] D. P. Adams and S. M. Yalisove, J. Appl. Phys. **76**, 5185 (1994).
[37] D. R. Hamann, Phys. Rev. Lett. **60**, 313 (1988).
[38] J. M. Gibson, J. L. Batstone, and R. T. Tung, Appl. Phys. Lett. **51**, 45 (1987).
[39] R. T. Tung and F. Schrey, J. Cryst. Growth **95**, 455 (1989).